ACS APPLIED MATERIALS & INTERFACES

Research Article

www.acsami.org

Nanoplasmonic Chitosan Nanofibers as Effective SERS Substrate for Detection of Small Molecules

Alexandra N. Severyukhina,[†,⊥] Bogdan V. Parakhonskiy,[†,‡,⊥] Ekaterina S. Prikhozhdenko,[†] Dmitry A. Gorin,[†] Gleb B. Sukhorukov,[§] Helmuth Möhwald,[∥] and Alexey M. Yashchenok*[,†,∥]

[†]Remote Controlled Theranostic Systems Lab, Institute of Nanostructures and Biosystem, Saratov State University, Saratov, 410012 Russia

[‡]A.V. Shubnikov Institute of Crystallography RAS, Moscow, 119333 Russia

[§]School of Engineering and Materials Science, Queen Mary University of London, Mile End Road, London, E1 4NS, U.K.

[∥]Max-Planck Institute for Colloids and Interfaces, Potsdam, 14424 Germany

Supporting Information

ABSTRACT: The use of surface enhanced Raman spectroscopy (SERS) is limited by low reproducibility and uniformity of the response. Solving these problems can turn the laboratory use of SERS into real-world application. In this regard, soft SERS-active substrates can enable portable instrumentation and reduce costs in the fabrication of SERS-based sensors. Here, plasmonic free-standing films made of biocompatible chitosan nanofibers and gold nanoparticles are engineered by a simple protocol varying the concentration of chloroauric acid. The concentration and distribution of gold nanoparticles in films are controlled in a predictable way, and SERS spectra for the standard 2-naphthalenethiol with concentration less than 10^{-15} M are acquired in a reproducible way. The statistical analysis reveals a relatively high and locally uniform performance of SERS with an enhancement factor of 2×10^5 for 86% of the points on the imaged area of the SERS substrate. Potential SERS detection of small molecules, both Rhodamine 6G and D-Glucose, in the micromolar range is demonstrated.

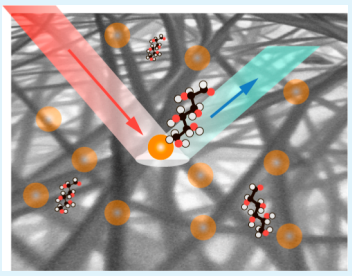

KEYWORDS: *SERS, chitosan nanofibers, gold nanoparticles, Rhodamine 6G, D-Glucose*

INTRODUCTION

Organizing plasmonic nanoparticles, in particular gold and silver, in arrayed nanoscale structures has received tremendous attention during the last 25 years.[1] This research direction termed "plasmonics" implies the creation of nanoscale systems with tunable optical properties and application in optics,[2] electronics,[3] biodiagnostic,[4] and medicine.[5] Several approaches such as chemical functionalization,[6] self-assembly of plasmonic nanoparticles,[7] and lithography techniques[8] have been used to design plasmonic nanostructures. To date, a number of these nanostructures have been obtained by impregnation of gold and silver nanoparticles on glass, quartz, and silicon substrates.[9] These substrates have been used to control the localized surface plasmon resonance (LSPR) of plasmonic nanoparticles and to create highly sensitive sensors, in particular by surface enhanced Raman scattering (SERS).[10−13] SERS has emerged as a powerful analytical technique for probing single molecules,[14,15] ions,[16] biomolecules,[17] and for cell studies.[18,19] In spite of the achievements of using rigid substrates as SERS sensors one needs to design systems that can be applied outside a specialized laboratory. Flexible plasmonic substrates, such as polymer nanofibers and cellulose paper, are a new class of plasmonic materials with low cost for fast diagnostics.[20] Compared to rigid-substrates, flexible structures are adaptable to a rough substrate in terms of wrapping and bending.[21] Furthermore, flexible plasmonic substrates open the perspective of combination with electronic components to generate a new class of multifunctional devices.[22] Electrospinning polymer nanofibers may yield nonwoven membranes of large-scale dimension with high surface area to volume ratio and elasticity. These peculiarities are of importance for the fabrication of functional and smart nanostructured materials.[23] Incorporation of silver nanoparticles in electrospun polymer nanofibers provides enhanced functionality and exhibits excellent anti-bacterial performance.[24] Hierarchical electrospun polymer films have been engineered with improved parameters required for SERS application,[25] and to date, there are two approaches to achieve functionality of electrospun nanofibers. The first is the incorporation of either a metal salt or as-prepared plasmonic nanoparticles in a polymer, and then a mixture is spun to achieve modification of nanofibers.[26,27] The second approach is based on the functionalization of the surface of polymer nanofiber substrates. For SERS, the latter approach seems very promising for detection of molecules without need to deposit molecules on "hot spots" located within polymer nanofibrous films. This approach has been established acquiring Raman signals of analytes adsorbed on polymer nanofibers decorated with silver nanoparticles.[28] To date, only few approaches show

Received: April 30, 2015
Accepted: June 30, 2015
Published: June 30, 2015

DOI: 10.1021/acsami.5b03696
ACS Appl. Mater. Interfaces 2015, 7, 15466−15473

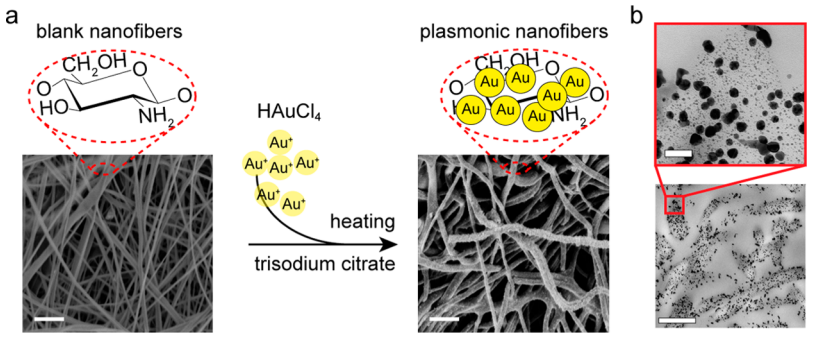

Figure 1. (a) Schematics showing functionalization of electrospun chitosan nanofibers with gold nanoparticles by immersion of as-prepared chitosan nanofibers in a selected concentration of chloroauric acid for 30 min and subsequently initiated gold nanoparticle growth by adding 1% trisodium citrate at 90 °C. SEM images of (left) as-prepared chitosan nanofibers and (right) those after functionalization. The scale bars in the SEM images correspond to 2 μm. (b) TEM image recorded by means of microtome cutting of chitosan fibers with embedded gold nanoparticles. Black dots point to the presence of gold nanoparticles. The scale bars in the TEM images correspond to (bottom) 500 nm and (top) 50 nm.

modification of polymer nanofibers based on in situ growth of plasmonic nanoparticles.[21,29] Decreasing the number of steps in preparation of plasmonic polymer nanofibrous films would assist in reducing the costs of samples. In addition, immediate decoration of polymer nanofibers would improve the characteristics of these structures, in particular to control their optical properties in a predictable manner. The latter is of paramount importance for the development of extremely sensitive and reproducible SERS sensors. In this regard, immediate modification of polymer nanofiber substrates with plasmonic nanoparticles is very promising for the construction of novel functional systems. In this work, we demonstrate an approach of fabricating plasmonic polymer nanofibrous substrates made of chitosan and gold nanoparticles. In the first stage, chitosan nanofibrous films are fabricated by electrospinning. Then polymer nanofibers are immersed into gold metal salt to contact Au ions with chemical groups of chitosan. In the final step, after immersion in chloroauric acid ($HAuCl_4$) solution, a modified Frens method is applied to initiate the growth of gold nanoparticles in chitosan nanofibers.[30] Compared to previously reported approaches of in situ impregnation of metal nanoparticles within electrospinning nanofibers, our study demonstrates (1) high yield of gold nanoparticles in chitosan nanofiber films; (2) a reduced number of steps required for sample preparation; and (3) control of the distribution of gold nanoparticles in nanofibers via the concentration of chloroauric acid.

In addition, the use of chitosan as a biocompatible natural polymer opens up possibilities to construct biocompatible functional nanofibrous materials with controlled plasmonic properties.

EXPERIMENTAL SECTION

Materials. Gold(III) chloride trihydrate ($HAuCl_4$), trisodium citrate dihydrate ($Na_3C_6H_5O_7$), poly(ethylene oxide) (PEO, 1000 kDa), D-(+)-Glucose ($C_6H_{12}O_6$, 180.16 Da, ≥99.5%), Rhodamine 6G (dye content ~95%, 479.01 Da) were purchased from Sigma-Aldrich. Chitosan (200 kDa, 80−85% degree of deacetylation) was purchased from Joint-Stock Company "Bioprogress" (Russia). In all experiments, ultrapure water with resistivity higher than 18.2 MΩ cm was used.

Synthesis of Electrospinning Nanofibrous Membranes. Chitosan and poly(ethylene oxide) with ratio of 93/7 were prepared by mixing under vigorous stirring for 2 h. Before that, chitosan (6% w/v) and PEO (1% w/v) solutions were prepared separately by dissolving chitosan or PEO powder in 70% acetic acid. Nonwoven chitosan nanofibers were produced utilizing a needle-free laboratory device for textile electrospinning, the NanoSpider NS 200 (Elmarco, Czech Republic). The distance between the four-wire rotating spinning electrode and the collecting electrode was 150 mm, the applied voltage was set to 80 kV.

Fabrication of Plasmonic Nanofibrous Films. To produce plasmonic chitosan nanofiber substrates, as-prepared blank nanofibers were immersed into water solution of chloroauric acid ($HAuCl_4$) with selected molar concentration. The chitosan nanofibers were left for 30 min to ensure binding of gold ions to chemical groups of chitosan. During adsorption the fibers turned yellow. After the adsorption procedure, the nanofiber films were washed several times with water to remove unbounded chloroauric acid. Then the substrates were placed in 5 mL heated water (90 °C) and 0.5 mL 1% trisodium citrate was added immediately to water containing fibers, and the mixture was left to stir for 10 min. After approximately 5 min of stirring, the chitosan nanofiber films changed color from yellow to slightly pink and then to deep red. This point indicates gold nanoparticle growth initiated by trisodium citrate as previously reported and employed by Frens.[30] Then the solution was brought to room temperature, and chitosan nanofibers decorated with gold nanoparticles were removed from the reaction vessel and washed several times with clean water.

Characterization. Scanning electron microscopy (SEM) images were recorded by means of a Philips XL30 electron microscope at an accelerating voltage of 3 kV. Field emission environmental electron microscopy (ESEM) was performed with a high-resolution low-vacuum FEI Quanda 600 FEG instrument at an operating voltage 30 kV with extended low-vacuum capabilities. Transmission electron microscopy (TEM) images were obtained on a Zeiss EM912 Omega transmission electron microscope at an operating voltage of 300 kV. To perform Raman measurements, we used two confocal microscopes. The first system is a confocal Raman microscope (CRM200, WITec, Ulm, Germany) equipped with a piezo-scanner (P-500, Physik Instrumente, Karlsruhe, Germany) and a diode-pumped 785 nm NIR laser excitation (Toptica Photonics AG, Graefelfing, Germany). The laser beam was focused through a 10× (Nikon, NA = 0.25) microscope objective. The spectra were acquired with a thermoelectrically cooled CCD detector (DU401ABV, Andor, U.K.) behind a grating (300 g mm^{-1}) spectrograph (Acton, Princeton Instruments, Inc., Trenton, NJ) with a spectral resolution of 6 cm^{-1}. The ScanCtrlSpectroscopyPlus software (version 1.38, Witec) was used for measurement and WITec Project Plus (version 2.02, Witec) for spectra processing.

The second is a confocal Raman microscope (Renishaw inVia, UK) equipped with a diode-pumped 785 nm NIR laser excitation (60 mW) controlled by a neutral optical density filter. The laser beam was focused through a 50× (Leica N PLAN, NA = 0.5) microscope objective. The spectra were acquired with a thermoelectrically cooled CCD detector optimized for near IR (spectral resolution of 1 cm^{-1}). All spectra were collected by using WiRE software V4.1 (Renishaw, U.K.) and SynchroScan was applied for processing of spectra. The

DOI: 10.1021/acsami.5b03696
ACS Appl. Mater. Interfaces 2015, 7, 15466−15473

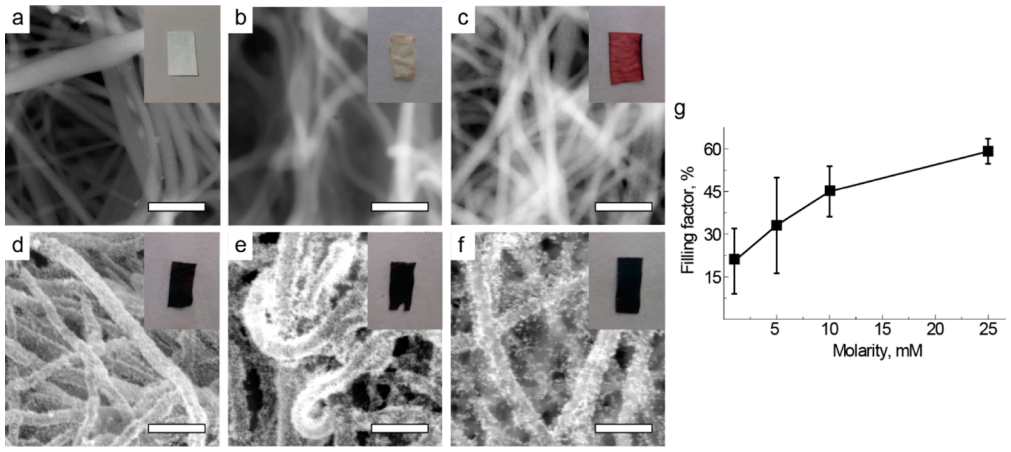

Figure 2. SEM images of (a) as-prepared chitosan nanofibers and chitosan nanofibers treated with $HAuCl_4$ at concentrations of (b) 0.5, (c) 1, (d) 5, (e) 10, and (f) 25 mM for 1 h, subsequent gold nanoparticle growth by adding 1% trisodium citrate. (g) Filling factor of gold nanoparticles versus molar concentration of chloroauric acid, estimated from SEM image analysis. The error bars are standard deviations (SD) of filling factor estimated in selected areas of one single fiber. All SEM images were obtained at the backscattered electron mode (BSEM). The insets are optical images of chitosan nanofiber films. The scale bars in the SEM images are 500 nm.

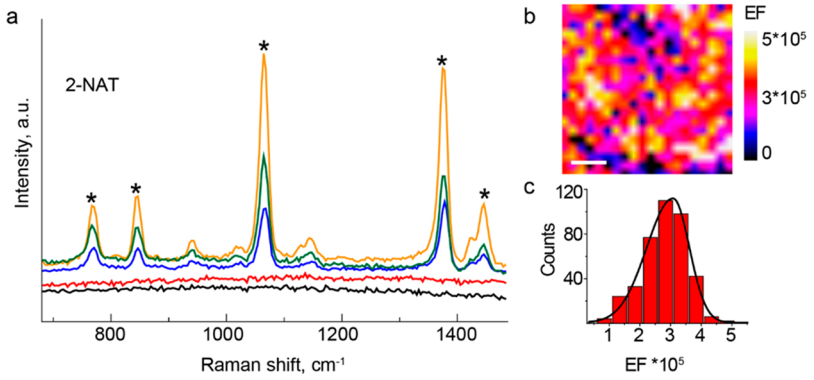

Figure 3. (a) SERS spectra of dried 2-NAT taken after casting 10 μL of its ethanol solution (10^{-3} M) on functionalized chitosan substrates prepared at a selected amount of chloroauric acid: (black) 0.5, (red) 1, (blue) 5, (orange) 10, and (green) 25 mM. The characteristic SERS peaks of 2-NAT centered at 763, 842, 1064, 1378, and 1452 cm^{-1} are marked with an asterisk. (b) Enhancement factor (EF) map calculated based on acquiring the Raman intensity at 1378 cm^{-1} and eq 2. (c) Histogram of an enhancement factor from the EF map. The scale bar on the EF map corresponds to 2 μm. SERS spectra were acquired through a 50× microscope objective using 785 nm light (0.03 mW) and an integration time of 10 s.

laser power was measured by a power meter (Newport Optical Power Meter 1830-C) before the microscope objective.

All SERS spectra were acquired from seven randomly selected points on a sample, and each curve is a mean curve. To examine reproducibility, we obtained three different batches of SERS substrates for each concentration of chloroauric acid. The WiRE software V4.1 (Renishaw, U.K.) and SynchroScan were used for spectra processing. We used a baseline correction tool in the WiRE software V4.1 (Renishaw, U.K.). The relative standard deviation (RSD) was estimated according to the following equation: RSD = (SD/I^m), where SD corresponds to the standard deviation of the Raman intensity and I^m is the mean Raman intensity of a specific peak.

Image Analysis. Analysis of SEM images was done by using ImageJ software (http://rsb.info.nih.gov/ij/). Selected areas of chitosan nanofiber substrates on SEM images were chosen to count the gold nanoparticles. We defined areas that are in one plane to ensure homogeneous distribution of gold nanoparticles. The filling factor was considered as particle cross section divided by the cross section of the polymer nanofiber film in randomly selected areas of polymer nanofiber mats. The size of the area cross section of polymer mats is considered equal to a laser spot size (1.8 μm). For each sample a minimum of five images were counted.

RESULTS AND DISCUSSION

To functionalize electrospun chitosan nanofibers with gold nanoparticles, we applied a two-stage procedure. First chitosan substrates 1 × 1 cm are saturated with Au ions from water solution of chloroauric acid (Figure 1). Here, Au ions are bound to the amino groups of the chitosan network. In the second stage, reduction of gold ions to the metallic nanoparticles is achieved by injection of citrate solution. The surface of the nanofibers undergoes changes after the modification, as shown in Figure 1. The gold nanoparticles cover the surface of nanofibers and make it thicker compare to blank substrates (Figure 1a, right-hand side SEM image). The alteration of the nanofiber surface can be seen more clearly on the SEM images obtained at the backscattered electron mode (Figure 2). Note that the color of the chitosan nanofibrous films changes to deep red compared to the blank sample (insets in Figure 2). TEM image analysis of substrates prepared at high concentration of chloroauric acid (25 mM) show plenty of gold nanoparticles in chitosan nanofibers (Figure 1b, overview). One can also claim that gold nanoparticles are located both within nanofibers and on their surfaces. We find that two sizes of gold colloids are grown in chitosan substrates. Tiny gold nanoparticles with a

DOI: 10.1021/acsami.5b03696
ACS Appl. Mater. Interfaces 2015, 7, 15466−15473

diameter of approximately 4 nm, and large colloids with an average diameter of 20 nm (Figure 1b, magnified TEM image). Due to the dense structure of the chitosan substrates both as-prepared and those after functionalization with gold nanoparticles, it is not trivial to apply UV−vis spectroscopy. However, one can predict the shift of the surface plasmon peak to the red part of the visible spectrum from purple (low amount $HAuCl_4$) to dark purple (high amount $HAuCl_4$; Figure 2). Note that SEM images were obtained at the backscattered electron mode (BSEM). This mode provides relatively high contrast of atomic numbers of elements, in our case, between gold nanoparticles and chitosan nanofibers. As a result, the images have relatively higher contrast compared to those obtained at the secondary electron mode. To assess the influence of the concentration of chloroauric acid on the quantities of gold nanoparticles in chitosan substrates, different concentrations of chloroauric acid were taken. We find that 0.5 mM of chloroauric acid is not enough to achieve a sufficient number of gold nanoparticles in chitosan nanofibers. It is suggested that at this concentration of chloroauric acid only small gold seeds (~4 nm) are grown (Figure 1b, enlarged TEM image). We observe only bright contrast in the SEM images for this type of samples compared to the blank one (Figure 2a,b). Starting from 1 mM concentration gold, nanoparticles appear in the chitosan nanofibers (Figure 2c). This sample did not exhibit reliable Raman signals during detection of the model reference 2-naphthalenethiol (Figure 3). Further increase of the metal salt concentration to 5, 10, and 25 mM showed plenty of gold nanoparticles distributed in the substrates (Figure 2d−f). To estimate the amount of gold nanoparticles in the films, we apply SEM image analysis. The number of gold nanoparticles can be expressed through the density of nanoparticles or surface filling factor:

$$F_S = \frac{\sum_i^n s_i}{S_f} = \frac{n\pi r_0^2}{Dh} \tag{1}$$

where s_i is the cross section of nanoparticles, S_f corresponds to surface of nanofiber, D is the diameter of the nanofiber, and h corresponds to the height of the nanofiber. The filling factor for all samples is expressed in percentage. We find that the concentration of chloroauric acid influences the distribution of gold nanoparticles in the chitosan substrates. The filling factor increases with molar concentration of chloroauric acid up to a value of 59% calculated for the samples prepared at 25 mM chloroauric acid (Figure 2g). Interestingly, the filling factor rises nearly linearly up to 10 mM of chloroauric acid concentration. The deviation at 5 mM of chloroauric acid is likely due to the nonuniform structure of nanofibrous films. As a result, the growth of gold nanoparticles appeared first in these irregularities forming gold clusters and then in single nanofibers. We further measure the influence of the concentration of chloroauric acid on the SERS signal of 2-naphthalenethiol (2-NAT). As mentioned above, low concentrations of chloroauric acid (0.5 mM and 1 mM) are not sufficient for a reliable SERS signal of 2-NAT.

However, several peaks of 2-NAT centered at 763 cm^{-1} (C−H wag), 1378, 1452 cm^{-1} (ring stretch), 842 cm^{-1} (C−H twist), 1064 cm^{-1} (symmetric C−H bending) are detected by casting ethanol solution on nanofibers with a high number of gold nanoparticles corresponding to 5, 10, and 25 mM of chloroauric acid (Figure 3a). New peaks appearing in the SERS spectrum at 842 cm^{-1} (C−H twist), 1064 cm^{-1} (symmetric C−H bending) are due to molecules chemisorbed on the surface of gold nanoparticles.[31] Our observation reveals that a higher SERS signal results from samples prepared at 10 mM chloroauric acid. On the contrary, the SERS signal acquired for the samples prepared at 25 mM chloroauric acid is reduced and appears similar to that of samples obtained at 5 mM chloroauric acid. We assume that this could be due to the higher number of gold nanoparticles in the substrates obtained at 10 mM chloroauric acid compared to 5 mM. As a result, high quantities of gold nanoparticles in these samples promote a sufficient amount of so-called "hot spots" that contribute to the SERS signal. Opposite to low concentration of chloroauric acid, for the higher concentration of chloroauric acid (25 mM) a large population of gold nanoparticles is observed (Figure 2g). However, this type of substrates does show further increase of the SERS and unenhanced Raman signal (which we call Raman signal) of 2-NAT comparable with samples prepared at 5 mM chloroauric acid. The attenuation of the Raman signal can be attributed to the shift of the surface plasmon peak to the red part of the visible spectrum.[32] At the same time, this can be induced by a decreasing number of "hot spots" due to the overgrowth of gold nanoparticles in chitosan nanofibers. For assessment of the efficiency of plasmonic chitosan nanofibers the enhancement factor (EF) was evaluated. We employ the averaged definition for SERS EF using the formula:

$$\mathrm{EF} = \left(\frac{\frac{I_{\mathrm{SERS}}}{N_{\mathrm{surf}}}}{\frac{I_{\mathrm{NR}}}{N_{\mathrm{vol}}}} \right) \tag{2}$$

where I_{SERS} and I_{NR} are SERS and (normal) Raman intensities (peak height at 1378 cm^{-1} from benzene ring stretching) acquired under identical conditions. N_{vol} and N_{surf} refer to the average number of molecules in the scattering volume for Raman and for SERS experiments. Assuming a molecular area of a 2-NAT molecule of approximately 0.22 nm^2, the surface concentration in a sampling area (N_{surf}) is about 8.5×10^6 molecules. The N_{vol} value was calculated to be 3.4×10^{13} in a sampling volume (laser spot size ~1.8 μm and penetration depth 3 μm). Thus, taking the molecular area of 2-NAT in the self-assembled monolayer into account and a vertical orientation on the surface of gold nanoparticles, the average enhancement factor is estimated to be 1.8×10^5. The enhancement factor was calculated only for the samples prepared at 10 mM chloroauric acid, as this sample showed a maximum SERS signal, when excited with a laser wavelength of 785 nm. The obtained value of the EF is in agreement with recently published data.[21,25] To verify the uniformity of the SERS signal from the developed plasmonic nanofibers, which is extremely important in terms of reproducibility, we performed confocal Raman imaging. Figure S1 (Supporting Information) represents a Raman image of 2-NAT at 1378 cm^{-1} on plasmonic chitosan nanofibers with an area of 10×10 μm^2.

We further calculate an enhancement factor for the imaged area by applying eq 2 (Figure 3b). The average EF calculated from the scanned area (400 points) is estimated to be 2.9×10^5 (SD 0.9×10^5) which is of the same order as the EF estimated for one single point of the plasmonic nanofibrous membrane. Nearly uniform EF distribution could be seen across the mapped area. A histogram with Gaussian fitting showed a normal distribution of the EF in the examined area (Figure 3c). We also find an enhancement factor higher than 2×10^5 for 86% of the nanofiber membrane. There are also areas with

DOI: 10.1021/acsami.5b03696
ACS Appl. Mater. Interfaces 2015, 7, 15466−15473

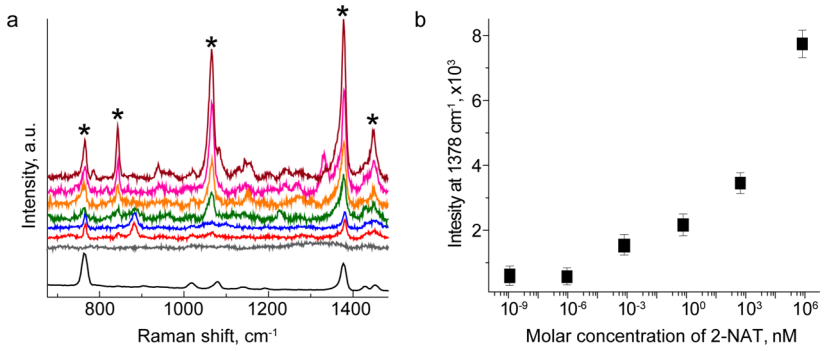

Figure 4. (a) Raman spectra of 2-naphthalenethiol as a powder (lower black curve), and SERS spectra of dried 2-naphthalenethiol taken by casting 10 μL of an ethanol solution with selected concentration (red, 10^{-18} M; blue, 10^{-15} M; green, 10^{-12} M; orange, 10^{-9} M; violet, 10^{-6} M; dark purple, 10^{-3} M; and gray, Raman spectrum of blank plasmonic nanofibers) on plasmonic chitosan nanofibers prepared at 10 mM concentration of chloroauric acid. The characteristic SERS peaks of 2-NAT centered at 763, 842, 1064, 1378, and 1452 cm^{-1} are marked with an asterisk. (b) Dependence of SERS intensity of the 1378 cm^{-1} peak against 2-NAT concentration. The error bars correspond to the standard deviation of the SERS intensity acquired from seven randomly selected positions. SERS spectra were collected through a 50× microscope objective using a laser with wavelength of 785 nm (0.03 mW) and an integration time of 10 s.

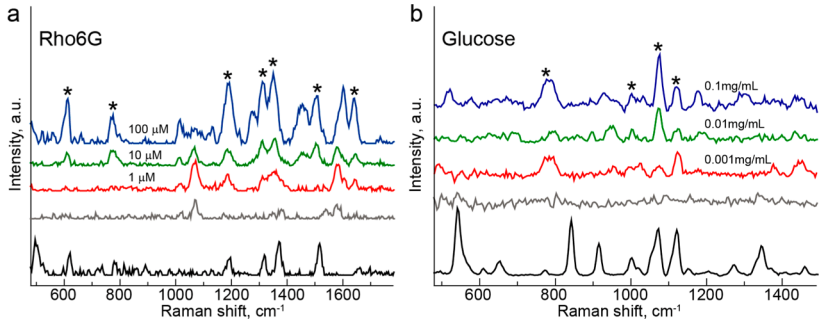

Figure 5. SERS spectra of Rhodamine 6G (a) and D-Glucose molecules (b) with varying concentrations. Asterisks mark the characteristic peaks of Rhodamine 6G and D-Glucose, respectively. Gray curves in both spectra correspond to the blank Raman spectra of the chitosan nanofibers. All SERS measurements were made using a laser with wavelength of 785 nm (10 mW for Rho6G and 0.5 mW for D-Glucose) and an integration time 3 s (a 10x microscope objective was used). Raman signals of Rhodamine 6G (water solution 1 mM) and D-Glucose (powder) were taken by operating at 785 nm (20 mW) and an integration time 10 s (lowest spectra).

relatively low EF intensities, likely due to the morphology of the chitosan nanofiber substrates that show interlaced stick-like structure and might be out of focus during the measurements. To investigate the capability of detection of low concentrated samples, Raman spectra were collected from plasmonic chitosan substrates obtained at 10 mM chloroauric acid. Because they have shown a maximal SERS signal of 2-NAT, this type of sample was taken at a laser wavelength of 785 nm. We use several concentrations of 2-NAT in ethanol solution. A reliable Raman signal of 2-NAT was acquired for all selected concentrations of 2-NAT. The samples showed a SERS signal at concentrations of 2-NAT up to 10^{-18} M (Figure 4a). Two basic peaks centered at 763 cm^{-1} (C−H wag) and 1378 cm^{-1} (ring stretch) are clearly seen in the spectra for all 2-NAT concentrations. These bands display a monotonous decay of the SERS intensity with lowering of the concentration of 2-NAT. A monotonic increase of the SERS intensity at 1378 cm^{-1} against concentration of 2-NAT was measured, as shown in Figure 4b. However, the increase of the SERS intensity with the concentration of 2-NAT is nonlinear. To clarify this, the chemical nature of 2-NAT and the surface chemistry of gold nanoparticles should be taken into account. There is a high affinity between 2-NAT (thiol groups in 2-NAT structure) and gold nanoparticles. By this hypothesis, the nonlinearity of the SERS intensity of 2-NAT could be explained with the assumption that at low analyte concentration, first the areas with high enhancement, like hot spots, are populated, and at higher concentrations those with lower field enhancement. On the other side, nonuniform coverage of the gold surface by the analyte and contributions of nonlocal effects are factors that can influence and reduce the SERS intensity.[33] To verify whether this type of substrate can enable reproducible SERS signals, those of 2-NAT were acquired from seven randomly selected points in the chitosan substrates under identical experimental conditions. From these measurements the relative standard deviation (RSD) of the major SERS bands was estimated to reveal SERS reproducibility. The RSD value of major SERS peaks of 2-NAT at selected concentrations is summarized in Table S1 (Supporting Information). We find that RSD values for major SERS peaks centered at 1064 cm^{-1}, 1378 and 1452 cm^{-1} are varying between 0.19 and 0.37 for concentrations of 2-NAT between 10^{-9} M to 10^{-18} M, respectively. At higher concentrations of 2-NAT (10^{-6} M), the RSD values are even raised to 0.5 for the SERS peak at 1064 cm^{-1}. These calculations indicate that the gold functionalized chitosan substrates have relatively high SERS reproducibility at low concentrations of 2-NAT.

The reproducibility of SERS signals obtained from three separate substrates were also evaluated. The RSD values of SERS intensities of the major peaks centered at 1064, 1378, and 1452 cm^{-1} were calculated to be 0.28.

DOI: 10.1021/acsami.5b03696
ACS Appl. Mater. Interfaces 2015, 7, 15466−15473

Subsequently, gold nanoparticle functionalized chitosan nanofibrous films were used for label-free detection of other molecules, namely Rhodamine 6G (Rho 6G) and D-Glucose. The latter is of paramount importance because it indicates the level of glucose in blood and serves as a biomarker of diabetes.[34] Figure 5 presents SERS spectra of Rho6G and D-Glucose taken from gold functionalized chitosan nanofibers. To obtain SERS of Rho6G spectra gold modified chitosan nanofibers were immersed into an aqueous Rhodamine solution (0.05 mL) of defined concentrations. After several minutes being immersed into Rhodamine solution SERS spectra were acquired from wet chitosan nanofiber substrates. To obtain D-Glucose spectra gold functionalized substrates were incubated into glucose solution for 1 h, followed by washing with pure water. SERS spectra were measured from dried chitosan nanofibers. Several Raman scattering modes of Rhodamine and D-Glucose are summarized in Table 1. SERS bands were

Table 1. Assignments of Raman and SERS Peaks of Rhodamine 6G and Glucose

Raman peak position (cm^{-1})	SERS peak position (cm^{-1})	assignments
	Rhodamine 6G	
614	613	in-plane bending of C−C−C ring
775	775	out-plane bending of C−H
1195	1193	in-plane bending of C−H
1317	1314	stretching of arom C−C
1370	1360	stretching of arom C−C
1515	1510	stretching of arom C−C
1650	1642	stretching of arom C−C
	glucose	
771	775	bending mode of (O_5−C_1-O_1)
1001	1001	rocking mode of CH_2
1071	1075	stretching mode C−H
1120	1120	bending mode of C−O−H

analyzed and compared with the Raman peaks of Rhodamine 6G and glucose collected in our study as well as with those that had been obtained by other groups.[35−37] For Rhodamine in the region between 600 and 1700 cm^{-1} the peaks which are due to bending in-plane and out-plane of C−H and stretching modes of the carbon skeleton remain almost unchanged. The four SERS bands centered at 1314, 1360, 1510, and 1642 cm^{-1} differ from the original Raman signal of Rhodamine 6G. All those strong bands are attributed to stretching of aromatic C−C, and the difference can be associated with the interaction between the surface of gold nanofibers and adsorbed Rhodamine. In addition, this can be partly attributed to reabsorption of the Stokes-shifted scattering, in particular for the sample with highest concentration (100 μM, Figure 5a).

Several peaks were observed in the SERS spectra of glucose, which are in the region between 700 and 1200 cm^{-1}. Only two bands centered at 775 and 1175 cm^{-1} slightly differ from that of the Raman spectrum of glucose. As mentioned above, glucose is a biomarker of diabetes, and therefore its detection with high efficacy is desirable. In our experiments, we were able to measure glucose in the range 1 μg/mL to 1 mg/mL. This range covers the glucose level for a normal person (<70−150 mg/mL), while for diabetics, the level is approximately above 150 mg/mL.[34] Our SERS-based detection of glucose reveals a high sensitivity even at 1 μg/mL. It is also worth mentioning that 1 μg/mL is the lowest value that can be detected by these SERS substrates. Note that glucose has plenty of hydroxyl groups, which might be protonated, and therefore it may have some influence on the pH of the solution. However, in our experiments the pH of the glucose solution was measured to be 6.9.

The RSD values were estimated for major SERS peaks of Rho 6G and D-Glucose at selected concentrations (Tables S2 and S3, Supporting Information). In the case of Rho 6G, the RSD values of the SERS intensity of major peaks do not exceed 0.3, revealing relatively good SERS reproducibility across the entire area of modified chitosan substrate. For glucose, the RSD values of the SERS intensity at 775 and 1075 cm^{-1} are observed to be below 0.25 at a concentration of 0.1 mg/mL.

A control experiment for the blank chitosan nanofiber (gray lines, Figure 5) reveals the dominance of only few lines for the nanofibers measured at the wet state (1067 and 1577 cm^{-1}). These bands can be attributed to the C−OH stretching and C−N vibration of chitosan. We attribute this to the fact that the chitosan substrates can undergo swelling upon immersion in water. At such a state, gold colloids can interact stronger both with neighboring nanoparticles and with the chitosan network than in dry condition. In addition, interaction between single adjacent nanofibers can take place and therefore contribute to the resultant SERS signal. Oppositely at dry state peaks that correspond to chitosan are not visible. It can be attributed to the relatively high amount of gold nanoparticles (TEM image) located on the surface of the substrates rather than within nanofibers. These nanoparticles can contribute significantly to the SERS signal compared to that of nanoparticles situated in the volume of the nanofibers. As a result, the contribution from impurities in chitosan substrates to the SERS signal would be minimal. Note that the citrate peaks, usually centered at 810, 842, 952, 1046, 1095, and 1412 cm^{-1}, were resolved in SERS measurements.

We have shown here a facile way of forming a nonwoven plasmonic substrate that is suitable to detect analytes with high sensitivity. In the specific case of glucose sensing, we would be able to reduce the laser intensity by a factor of 40 to be able to distinguish between healthy or diabetics. Thus, we can make use of the high specificity of Raman detection, but with rather cheap technology in a portable device.

CONCLUSIONS

In conclusion, we have introduced an approach of in situ fabrication of plasmonic substrates by using bicompatible free-standing electrospun chitosan nanofibers. These substrates can be prepared by first immersing them into solution of chloroauric acid and subsequently initiating the growth of gold nanoparticles by adding trisodium citrate in heated water. The distribution of gold nanoparticles in chitosan nanofibers can be controlled by changing the concentration of chloroauric acid. This plasmonic chitosan nanofibrous substrate displays effective SERS detection of the standard 2-NAT of a concentration less than 10^{-15} M. The SERS performance is examined by applying confocal Raman imaging on the plasmonic chitosan nanofiber films. Only 14% of the points in the plasmonic nanofibrous membrane have an enhancement factor less than 2×10^5. Potential detection of Rhodamine 6G and an important biomarker of diabetes, D-Glucose, was shown. A reliable SERS signal is achieved in the concentration range of micrometers (μM) for both molecules. The approach demonstrated in this paper possesses perspectives for efficient and scalable functionalization of plasmonic substrates along

DOI: 10.1021/acsami.5b03696
ACS Appl. Mater. Interfaces 2015, 7, 15466−15473

with the control of their optical properties. Furthermore, the developed SERS plasmonic electrospun substrates open up possibilities integrating them with conventional techniques such as chromatography and microfluidics. The latter intends to improve the detection of complex samples with high efficiency, reproducibility, and selectivity and makes the SERS analytical technique a powerful tool in conventional medical diagnostics.

■ ASSOCIATED CONTENT

Supporting Information

Optical image of plasmonic nanofibrous films, reconstructed Raman image. The Supporting Information is available free of charge on the ACS Publications website at DOI: 10.1021/acsami.5b03696.

■ AUTHOR INFORMATION

Corresponding Author

*Email: alexey.yashchenok@mpikg.mpg.de.

Author Contributions

⊥These authors contributed equally. A.N.S. and E.S.P. synthesized chitosan nanofibers, conducted their functionalization by gold nanoparticles, conducted Raman measurements and contributed to writing of the manuscript; B.V.P. performed images analysis and contributed to writing of the manuscript; D.A.G., G.B.S., H.M., and A.M.Y. designed the experiments and contributed to writing of the manuscript.

Notes

The authors declare no competing financial interest.

■ ACKNOWLEDGMENTS

The study was supported by the Government of the Russian Federation (grant no. 14.Z50.31.0004 to support scientific research projects implemented under the supervision of leading scientists at Russian institutions and Russian institutions of higher education). The study was partly supported by RFBR research project no. 15-29-01172 ofi_m.

■ REFERENCES

(1) Atwater, H. The Promise of Plasmonics. *Sci. Am.* **2007**, *296*, 56−63.

(2) Ai, B.; Yu, Y.; Möhwald, H.; Zhang, G. Responsive Monochromatic Color Display Based on Nanovolcano Arrays. *Adv. Opt. Mater.* **2013**, *1*, 724−731.

(3) Atwater, H.; Polman, A. Plasmonics for Improved Photovoltaic Devices. *Nat. Mater.* **2010**, *9*, 205−213.

(4) Khlebtsov, N.; Bogatyrev, V.; Dykman, L.; Khlebtsov, B.; Staroverov, S.; Shirokov, A.; Matora, L.; Khanadeev, V.; Pylaev, T.; Tsyganova, N.; Terentyuk, G. Analytical and Theranostic Applications of Gold Nanoparticles and Multifunctional Nanocomposites. *Theranostics* **2013**, *3*, 167−180.

(5) Shen, H.; You, J.; Zhang, G.; Ziemys, A.; Li, Q.; Bai, L.; Deng, X.; Erm, R.; Liu, X.; Li, C.; Ferrari, M. Cooperative, Nanoparticle-Enabled Thermal Therapy of Breast Cancer. *Adv. Healthcare Mater.* **2012**, *1*, 84−89.

(6) Yu, X.; Lei, Y.; Amin, F.; Hartmann, R.; Acuna, P.; Guerrero-Martínez, A.; Maier, A.; Tinnefeld, P.; Carregal-Romero, S.; Parak, W. Distance Control in-between Plasmonic Nanoparticles via Biological and Polymeric Spacers. *Nano Today* **2013**, *8*, 480−493.

(7) Klinkova, A.; Choueiri, R. M.; Kumacheva, E. Self-Assembled Plasmonic Nanostructures. *Chem. Soc. Rev.* **2014**, *43*, 3976−3991.

(8) Merk, V.; Kneipp, J.; Leosson, K. Gap Size Reduction and Increased SERS Enhancement in Lithographically Patterned Nanoparticle Arrays by Templated Growth. *Adv. Opt. Mater.* **2013**, *1*, 313−318.

(9) Schweikart, A.; Pazos-Pérez, N.; Alvarez-Puebla, R.; Fery, A. Controlling Inter-Nanoparticle Coupling by Wrinkle-Assisted Assembly. *Soft Matter* **2011**, *7*, 4093−4100.

(10) Kleinman, S.; Frontiera, R.; Henry, A.-I.; Dieringer, J.; Van Duyne, R. Creating, Characterizing, and Controlling Chemistry with SERS Hot Spots. *Phys. Chem. Chem. Phys.* **2013**, *15*, 21−36.

(11) Parakhonskiy, B.; Svenskaya, Y.; Yashchenok, A.; Fattah, H.; Inozemtseva, O.; Tessarolo, F.; Antolini, R.; Gorin, D. Size Controlled Hydroxyapatite and Calcium Carbonate Particles: Synthesis and Their Application as Templates for SERS Platform. *Colloids Surf., B* **2014**, *118*, 243−248.

(12) Cui, Q.; Yashchenok, A.; Zhang, L.; Li, L.; Masic, A.; Wienskol, G.; Möhwald, H.; Bargheer, M. Fabrication of Bifunctional Gold/Gelatin Hybrid Nanocomposites and Their Application. *ACS Appl. Mater. Interfaces* **2014**, *6*, 1999−2002.

(13) Yashchenok, A.; Borisova, D.; Parakhonskiy, B.; Masic, A.; Pinchasik, B.; Möhwald, H.; Skirtach, A. Nanoplasmonic Smooth Silica versus Porous Calcium Carbonate Bead Biosensors for Detection of Biomarkers. *Ann. Phys.* **2012**, *524*, 723−732.

(14) Rodríguez-Lorenzo, L.; Álvarez-Puebla, R.; Pastoriza-Santos, I.; Mazzucco, S.; Stéphan, O.; Kociak, M.; Liz-Marzán, L.; García De Abajo, J. Zeptomol Detection Through Controlled Ultrasensitive Surface-Enhanced Raman Scattering. *J. Am. Chem. Soc.* **2009**, *131*, 4616−4618.

(15) Khlebtsov, B.; Khanadeev, V.; Panfilova, E.; Bratashov, D.; Khlebtsov, N. Gold Nanoisland Films as Reproducible SERS Substrates for Highly Sensitive Detection of Fungicides. *ACS Appl. Mater. Interfaces* **2015**, *7*, 6518−6529.

(16) Li, J.; Chen, L.; Lou, T.; Wang, Y. Highly Sensitive SERS Detection of As 3 + Ions in Aqueous Media Using Glutathione Functionalized Silver Nanoparticles. *ACS Appl. Mater. Interfaces* **2011**, *3*, 3936−3941.

(17) Xu, L.; Zong, C.; Zheng, X.; Hu, P.; Feng, J.; Ren, B. Label-Free Detection of Native Proteins by Surface-Enhanced Raman Spectroscopy Using Iodide-Modified Nanoparticles. *Anal. Chem.* **2014**, *86*, 2238−2245.

(18) Yashchenok, A.; Masic, A.; Gorin, D.; Shim, B.; Kotov, N.; Fratzl, P.; Möhwald, H.; Skirtach, A. Nanoengineered Colloidal Probes for Raman-Based Detection of Biomolecules Inside Living Cells. *Small* **2013**, *9*, 351−356.

(19) Drescher, D.; Büchner, T.; McNaughton, D.; Kneipp, J. SERS Reveals the Specific Interaction of Silver and Gold Nanoparticles with Hemoglobin and Red Blood Cell Components. *Phys. Chem. Chem. Phys.* **2013**, *15*, 5364−5373.

(20) Polavarapu, L.; Liz-Marzán, L. Towards Low-Cost Flexible Substrates for Nanoplasmonic Sensing. *Phys. Chem. Chem. Phys.* **2013**, *15*, 5288−5300.

(21) Zhang, L.; Gong, X.; Bao, Y.; Zhao, Y.; Xi, M.; Jiang, C.; Fong, H. Electrospun Nanofibrous Membranes Surface-Decorated with Silver Nanoparticles as Flexible and Active/Sensitive Substrates for Surface-Enhanced Raman Scattering. *Langmuir* **2012**, *28*, 14433−14440.

(22) Qu, L.-L.; Li, D.-W.; Xue, J.-Q.; Zhai, W.-L.; Fossey, J.; Long, Y.-T. Batch Fabrication of Disposable Screen Printed SERS Arrays. *Lab Chip* **2012**, *12*, 876−881.

(23) Wu, J.; Wang, N.; Zhao, Y.; Jiang, L. Electrospinning of Multilevel Structured Functional Micro-Nanofibers and Their Applications. *J. Mater. Chem. A* **2013**, *1*, 7290−7305.

(24) Song, J.; Kang, H.; Lee, C.; Hwang, S.; Jang, J. Aqueous Synthesis of Silver Nanoparticle Embedded Cationic Polymer Nanofibers and Their Antibacterial Activity. *ACS Appl. Mater. Interfaces* **2012**, *4*, 460−465.

(25) Qian, Y.; Meng, G.; Huang, Q.; Zhu, C.; Huang, Z.; Sun, K.; Chen, B. Flexible Membranes of Ag-Nanosheet-Grafted Polyamide-Nanofibers as Effective 3D SERS Substrates. *Nanoscale* **2014**, *6*, 4781−4788.

(26) He, D.; Hu, B.; Yao, Q.; Wang, K.; Yu, S. Large-Scale Synthesis of Flexible Free- Sensitivity: Electrospun PVA Nanofibers of Silver Nanoparticles. *ACS Nano* **2009**, *3*, 3993−4002.

DOI: 10.1021/acsami.5b03696
ACS Appl. Mater. Interfaces 2015, 7, 15466−15473

(27) Inozemtseva, O.; Salkovskiy, Y.; Severyukhina, A.; Vidyasheva, I.; Petrova, N.; Metwally, H.; Stetciura, I.; Gorin, D. Electrospinning of Functional Materials for Biomedicine and Tissue Engineering. *Russ. Chem. Rev.* **2015**, *84*, 251−274.
(28) Bao, Y.; Lai, C.; Zhu, Z.; Fong, H.; Jiang, C. SERS-Active Silver Nanoparticles on Electrospun Nanofibers Facilitated via Oxygen Plasma Etching. *RSC Adv.* **2013**, *3*, 8998−9004.
(29) Yang, H.; Huang, C. Polymethacrylic Acid-Facilitated Nanofiber Matrix Loading Ag Nanoparticles for SERS Measurements. *RSC Adv.* **2014**, *4*, 38783−38790.
(30) Frens, G. Controlled Nucleation for the Regulation of the Particle Size in Monodisperse Gold Suspensions. *Nature, Phys. Sci.* **1973**, *241*, 20−22.
(31) Alvarez-Puebla, R.; Dos Santos, D., Jr; Aroca, R. Surface-Enhanced Raman Scattering for Ultrasensitive Chemical Analysis of 1 and 2-Naphthalenethiols. *Analyst* **2004**, *129*, 1251−1256.
(32) Pazos-Perez, N.; Wagner, C.; Romo-Herrera, J.; Liz-Marzán, L.; García De Abajo, J.; Wittemann, A.; Fery, A.; Alvarez-Puebla, R. Organized Plasmonic Clusters with High Coordination Number and Extraordinary Enhancement in Surface-Enhanced Raman Scattering (SERS). *Angew. Chem., Int. Ed.* **2012**, *51*, 12688−12693.
(33) García De Abajo, J. Nonlocal Effects in the Plasmons of Strongly Interacting Nanoparticles, Dimers, and Waveguides. *J. Phys. Chem. C* **2008**, *112*, 17983−17987.
(34) *Glucose Sensing, Topics in Fluorescence Spectroscopy, Vol. 11*, Edited by Geddes, C. D., Lakowicz, J. R.; Springer Science+Business Media, Inc.: New York, 006.
(35) Hildebrandt, P.; Stockburger, M. Surface-Enhanced Resonance Raman Spectroscopy of Rhodamine 6G Adsorbed on Colloidal Silver. *J. Phys. Chem.* **1984**, *88*, 5935−5944.
(36) Vasko, P.; Blackwell, J.; Koenig, J. Infrared and Raman Spectroscopy of Carbohydrates Carbohydr. *Carbohydr. Res.* **1971**, *19*, 297−310.
(37) Vasko, P.; Blackwell, J.; Koenig, J. Infrared and Raman Spectroscopy of Carbohydrates Carbohydr. *Carbohydr. Res.* **1972**, *23*, 407−416.

DOI: 10.1021/acsami.5b03696
ACS Appl. Mater. Interfaces 2015, 7, 15466−15473